ADVANCED INTELLIGENT SYSTEMS Open Access
www.advintellsyst.com

Ultralight Soft Wearable Haptic Interface with Shear-Normal-Vibration Feedback

*Jiyong Min, Seongkwan Jang, Seohu Lee, and Youngsu Cha**

Tactile information in virtual reality enhances immersion and realism by transferring physical stimuli to users. Therefore, the implementation of haptics in virtual environments has emerged as a significant issue. To achieve such tactile implementation, it is essential to develop wearable devices that provide various forms of physical stimulation without restrictions on movement. Herein, an ultralight device capable of delivering multiple tactile sensations, especially shear sensations, is developed through a novel pneumatic actuator and installable origami pump. In particular, this device with only 2 g has the ability to transmit normal forces, shear forces, and vibrations to the fingertips, thereby providing appropriate stimuli based on virtual environments. Moreover, by utilizing wearable and installable pneumatic sources via the origami pump, lightweight feedback is possible to operate independently without the need for an external air supply. Furthermore, our device is demonstrated in various virtual simulations with shear feedback. The novel haptic system is expected to serve as an interface between real users and virtual reality by incorporating multimodal sensations.

1. Introduction

Virtual reality has been developed to provide people with artificial experiences within educational, gaming, and healthcare environments.[1–3] In the same context, the development of virtual reality has led to an interest in wearable haptic devices to give people a vivid sense of immersion. The wearable devices can be utilized to control an avatar within the virtual reality and transmit information generated by physical phenomena between virtual objects to the users.[4–6] In particular, haptic cutaneous feedback devices express texture, weight, and softness of the objects in virtual reality, and also allow users to manipulate the virtual objects delicately.[7,8] For the bridge between the real world and virtual reality via these devices, it is critical to achieve complex physical senses using normal forces, shear forces, and vibration to imitate human sensation.[9–12] Specifically, as users interact with virtual objects through their hands, the wearable haptic device can be worn on the fingers and can replicate complex physical sensations.

To generate complex cutaneous feedback on the fingers from the device, mechanisms applying 3D vector forces have been typically used.[13] This mechanism transferred the cutaneous feedback through a platform that makes contact with the fingertip. The platform was controlled by the actuators to create the 3D forces. For example, generating sophisticated vibrations on the platform using voice coil actuators can provide a variety of tactile sensations for different textures and allow for a compact design of a wearable device.[14,15] In addition, employing servo motors or foam actuators in the haptic device enables the transfer of curved surface sensation to the user.[16,17] However, a rigid and robust case is required to fix actuators on the fingertips as one haptic device. This rigid case may cause discomfort for users. As users use their hands to perform intricate gestures or interact with objects, we considered the use of pneumatic actuators for comfortable wearing and reducing the electric components in haptic devices on the fingertips.

Recently, soft pneumatic actuators have attracted enormous attention as one of the haptic techniques applied in wearable devices for rendering the physical senses. The soft pneumatic actuator is typically made of inflatable soft materials and operates by applying positive relative pressure to the inner cavity of the actuator.[18] It is advantageous to configure the actuator in various shapes according to specific applications, as the inflation direction can be controlled by methods of inserting fabric materials or designing its structure.[19–22] By controlling inflation directions, these actuators can generate high force in a narrow area.[23] In addition, compared with other rendering technologies for physical sensations such as electrotactile, electromagnetic, dielectric elastomer, and piezoelectric, the soft pneumatic techniques are relatively inexpensive and lightweight.[24,25] Moreover, it is safe for users because there is no electronic device making contact with the skin. Despite these advantages, haptic devices using pneumatic actuators have several issues in this application. For providing sophisticated stimulation on the fingers, haptic devices should deliver multiple tactile feedback based on virtual simulations. Generally, one pneumatic actuator can perform one direction or motion. To provide multiple tactile feedback, including normal force, shear force, and vibration in various directions, several pneumatic actuators have to be integrated into one

J. Min, S. Jang, S. Lee, Y. Cha
School of Electrical Engineering
Korea University
145 Anam-ro, Seongbuk-gu, Seoul 02841, South Korea
E-mail: ys02@korea.ac.kr

The ORCID identification number(s) for the author(s) of this article can be found under https://doi.org/10.1002/aisy.202500374.

DOI: 10.1002/aisy.202500374

system.[20,26,27] In particular, a minimum of two pneumatic actuators is required to induce shear forces on the skin surface. By employing multiple actuators, shear forces could be applied to the wrist with considerable strength.[12,20,26,28] However, since the wrist-worn haptic device exceeds 50 mm in size or 50 g in weight, it is difficult to adapt to the fingertip. To overcome this limitation, some pneumatic actuators for finger-worn devices also have been developed. For example, a ring-type pneumatic actuator could produce forces up to 6.3 N and a frequency of 250 Hz with a weight of 4.5 g.[29] However, the force direction of this device was limited to one direction. In another case, a fingertip haptic device, which is foldable in various directions using origami methods, could produce a maximum of 7 N of normal force and 1.3 N of shear force, with a weight of 13.7 g.[30] When compared to these pneumatic finger-worn devices, we propose a novel haptic device design that reduces the form factor weight to 2 g in order to provide multiple tactile feedback, particularly for realizing the shear force.

With the new design that allows for multiple feedback, wearable devices should also consider the aspect of wearability. Wearability refers to how comfortable a user feels while wearing a device, without it restricting the movements of their hands; to meet this requirement, haptic gloves and electronic skin have been selected as an effective and user-friendly method.[31–34] These devices are lightweight and compact, making them comfortable to wear on the human.[35] Meanwhile, pneumatic systems typically require external sources of air pressure and valves that are usually bulky and heavy.[28,36,37] Similarly, most haptic devices needed external air sources to supply air pressure, and they must be connected to the air sources via tube lines.[12,20,26,28,30] Limitations on the actions of the user may occur due to the presence of these lines. To eliminate the limitations caused by the lines, pneumatic sources should also be lightweight and wearable. One of the methods is to use an origami technique.[38–41] The origami technique of folding a 2D structure into a 3D form is an effective method for producing multiple small pumps, owing to its lightweight characteristics and ease of expansion.[42,43] Pumps manufactured using origami techniques primarily operate through compression via a motor, returning to their original state due to their own elastic resilience.[44–46] Furthermore, the origami pump can generate air pressure through a simple folding action, eliminating the need for separate rotational components or valves. Thus, by combining pneumatic actuators with origami pumps, portable and wireless wearable devices can be designed. To incorporate these origami pumps into wearable devices, the appropriate size and weight of the pump with the motor should be considered in this system.

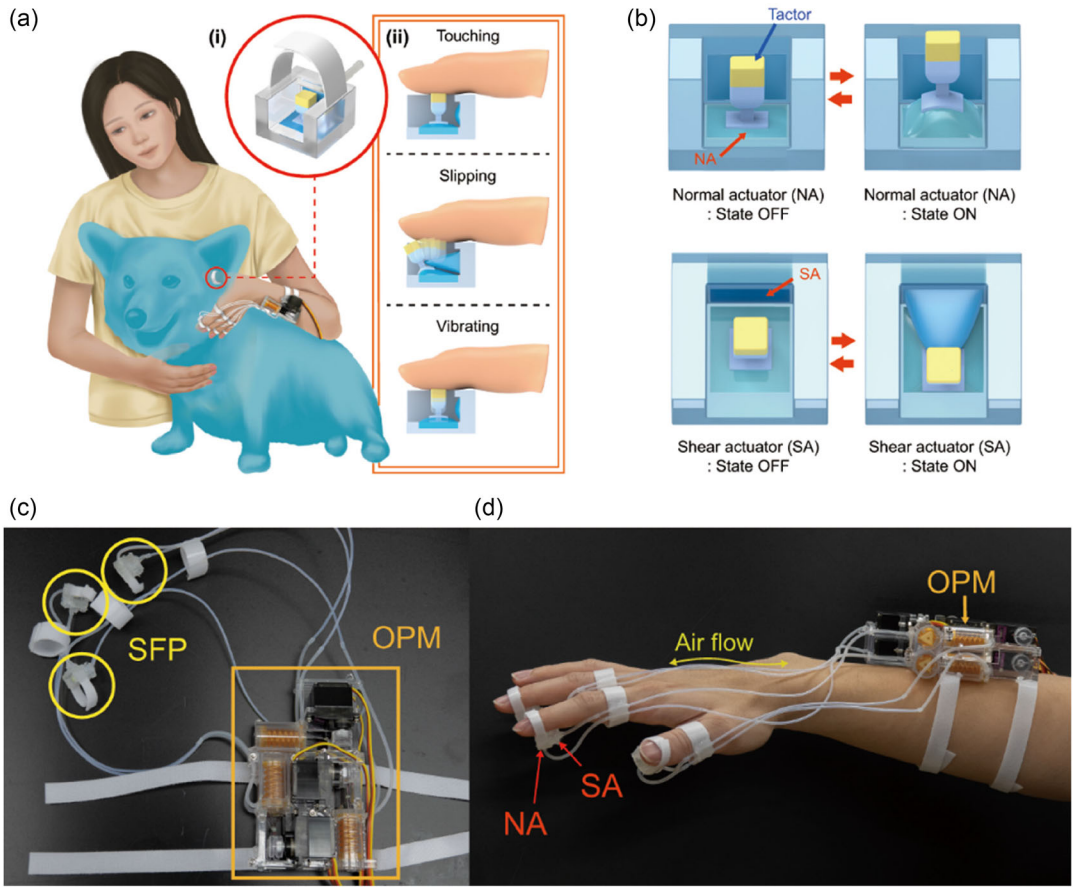

Figure 1. Overview of proposed wearable pneumatic haptic device system. a) Illustration of the application of the haptic device system. i) The overall structure of the device. ii) The multiple feedback, including touching, slipping, and vibrating. b) The operation states of the normal- and shear-direction actuators. c) Pictures of the SFP connecting with the OPM. d) Picture of wearing the device at the finger and forearm.

Herein, by applying the advantages of pneumatic actuators and devising a novel design suitable for fingertips, we propose a soft fingertip pneumatic device (SFP) with an origami pump module (OPM) to provide multiple tactile feedback (shear-normal-vibration). Specifically, a unique tactor displacement technique is utilized at the SFP to transmit tactile feedback.[47–50] As the tactor can freely move, it is capable of delivering normal and shear forces through two pneumatic actuators, a normal-direction actuator (NA) and shear-direction actuator (SA), as shown in **Figure 1**. By adjusting the operation time of these two actuators, the various types of feedback such as touching, slipping, and vibrating can be expressed on the fingertip, as illustrated in Figure 1a. Each actuator can operate independently, as illustrated in Figure 1b. The OPM, utilizing tendon-driven techniques, is designed as a single module that can be simply combined with multiple OPMs, and its compact size allows for it to be worn on the forearm, as shown in Figure 1c,d. When the OPM is attached to the forearm, it reduces the distance between the OPM and SFP without long tube lines. As a consequence, this device shows promise in implementing multiple tactile feedback through wearable technology in virtual reality.

2. Results

2.1. Generating Multiple Tactile Feedback

In virtual reality, tactile sensation is important to interact with virtual objects. Without tactile sensation, it is difficult to perceive distances between virtual objects and their hands, as humans typically rely on the sense of touch to control their behavior in relation to objects.[51,52] Specifically, the effective simulation of essential hand activities of daily lives within virtual reality environments, such as grasping and object manipulation, necessitates the design of normal force, shear force, and vibration feedback mechanisms.[53] Additionally, the receptive field area (average 0.055 cm^2) and the threshold force of mechanical receptors (0.57mN) to transmit stimuli to neurons should be considered when designing the haptic feedback device.[54] To satisfy these requirements, we fabricated a SFP to apply normal force, shear force, and vibration to the finger. The detailed fabrication process was described in the Experimental Section and Figure S7, Supporting Information.

With this fabricated SFP, OPMs were used to supply air pressure to the SFP. When the two OPMs were connected with two pneumatic actuators, each actuator could operate independently. From these two independent operations, a unique working principle was established to express various types of tactile feedback including touching, slipping, and vibrating, as shown in **Figure 2**a and Movie S1, Supporting Information. The movie presented how the SFP worked to generate these various forms of tactile feedback. Specifically, this principle consisted of four stages: 1) the actuators of SFP remain in a stationary state before contacting; 2) the NA expands to make the tactor reach the fingertip—by activating only the NA, the touch on the fingertip can be maintained continuously to deliver the virtual touching feeling to the user; 3) the expanding SA shifts the tactor forward—the SA is used to transfer the slipping feeling to the fingertip; and 4) the SA and NA are contracted, and the SFP returns to its initial state. Moreover, during this process, rapid pneumatic pressure changes can generate a vibrating feeling on the fingertip.

To validate this operation, we recorded actual movements of the black-painted tactor for tracking at a rate of 60 fps as shown in Figure 2b. In addition, the tactor movements were analyzed using a postprocessing tracking program (ProAnalyst Motion Analysis Software, Xcitex, Inc.). The trajectory of the tactor is demonstrated in Figure 2c. In this graph, a distance shifted forward was indicated by the x-axis, and a distance shifted vertically was indicated by the y-axis. The origin was the initial position of the tactor. Also, each point of the graph was the position of the tactor in a single frame of the tracking video. The red line in the graph represented the trajectory of the tactor moved according to our operation principle. From this graph, we confirmed that the tactor could move forward while maintaining the distance in the vertical direction. Moreover, the velocity of the tactor during horizontal movement was 8.325 mm s^{-1}, a value adequate for producing shear force in the tactor displacement method.[55,56] This indicated that the tactor could provide slipping feeling to the fingertip. However, when the NA shrank rapidly, the tactor might not deliver sufficient feeling to the fingertip. To prevent this, the shear extension method was performed. In the method, removing a portion of the pneumatic pressure from the NA allowed it to maintain a slightly inflated state, thereby preventing the tactor from suddenly detaching from the finger. The trajectory variation with this method was represented by a blue line in the graph of Figure 2c. We observed that the blue line from the shear extension method had more extended horizontal movement of the tactor increased by 10% compared to the red line. Additionally, despite rapid movements during repetitive actions, stable operation for sensory formation is demonstrated in Figure S1, Supporting Information. Therefore, the shear extension method was a more effective way to transfer shear force to the fingertip.

Furthermore, force measurements were conducted to examine magnitudes of normal and shear forces generated by the SFP. The experimental setup for the force measurements is demonstrated in Figure S2, Supporting Information. Figure 2d depicts the values of the normal and shear forces, along with the input pressure. From the graph, the maximum normal and shear forces of the SFP were 0.36 and 0.17 N, respectively. Despite the small forces, as an area in contact with the fingers of the tactor was small (16 mm^2), the SFP could deliver sufficient pressure for a user to feel cutaneous feedback.[57] Specifically, in haptic sensation, the shear force a person received could be transmitted differently depending on the normal force given in advance,[58,59] since the tactile forces transmitted to a person consisted of the resultant force formed by the combination of the normal forces and the shear forces generated by each actuator.[12,20] We confirmed from the force measurement that the SFP could deliver sufficient forces beyond the threshold of mechanical receptors. Thus, combining the two forces from the actuators appropriately, multiple feedback, including touching, slipping, and vibrating, could be demonstrated for various virtual simulations.

2.2. Designing Origami Pump Module for Wearable Device

When the SFP was operated, the NA and SA were supplied by the OPMs. Herein, to enhance the versatility of the wearable device,

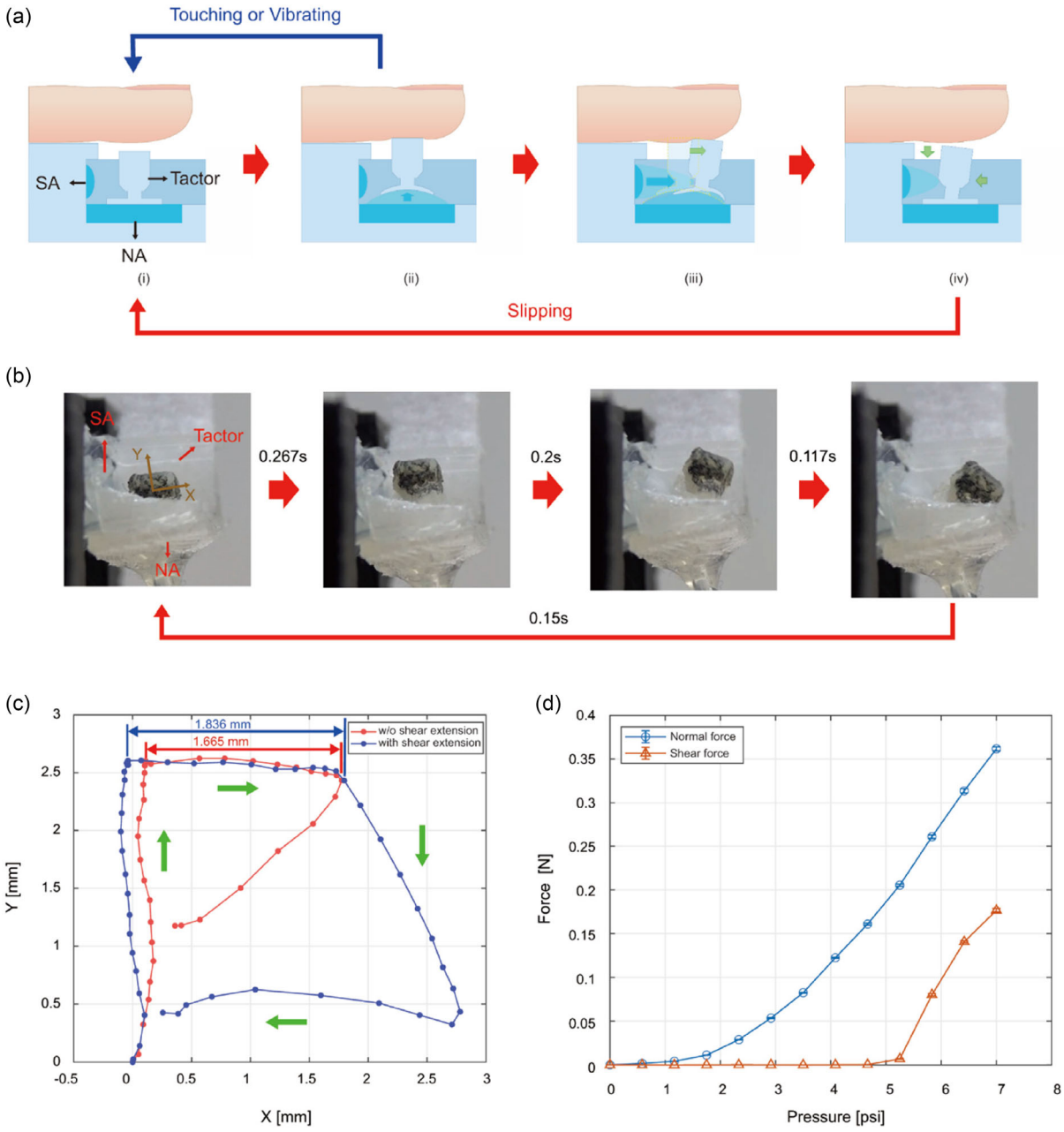

Figure 2. Motion and evaluation of the SFP. a) Schematic of the SFP working principles. b) Photographs of its working principles. The time above the arrows presented the operation time between each state for one cycle of 0.8 s. c) Tactor tracking depending on the presence or absence of middle actuation. The arrows indicated moving directions of the tactor. d) Measuring of blocking normal forces and blocking shear forces from the tactor. The error bars indicated standard deviation of 10 repetitions.

the size of the OPM must be minimized. For providing adequate force feedback with the minimum pump size, designing of the OPM proceeded. The origami pump operated using tendon-driven techniques, as illustrated in **Figure 3**a. To utilize the tendon-driven techniques, the Yoshimura origami pattern was selected for designing our pump, as the Yoshimura pattern can be axially contracted or extended.[60] The polyester thread was connected between the origami pump and a servo motor. The servo motor can be operated from 0° to 180° using a Pulse Width Modulation (PWM) method. When a microcontroller unit sent a signal with a frequency of 60 Hz, the duty cycle was varied between 0.6 and 2.4 ms, resulting in the servo motor rotating from 0° to 180°. Through the rotation of the motor, we controlled the contraction distance of the origami pump. The contraction distance increased linearly depending on the rotation angle after a tendon fastening stage, and it did not increase when the resilience force of the origami pump and tendon force were parallel.[61] With this tension transmission

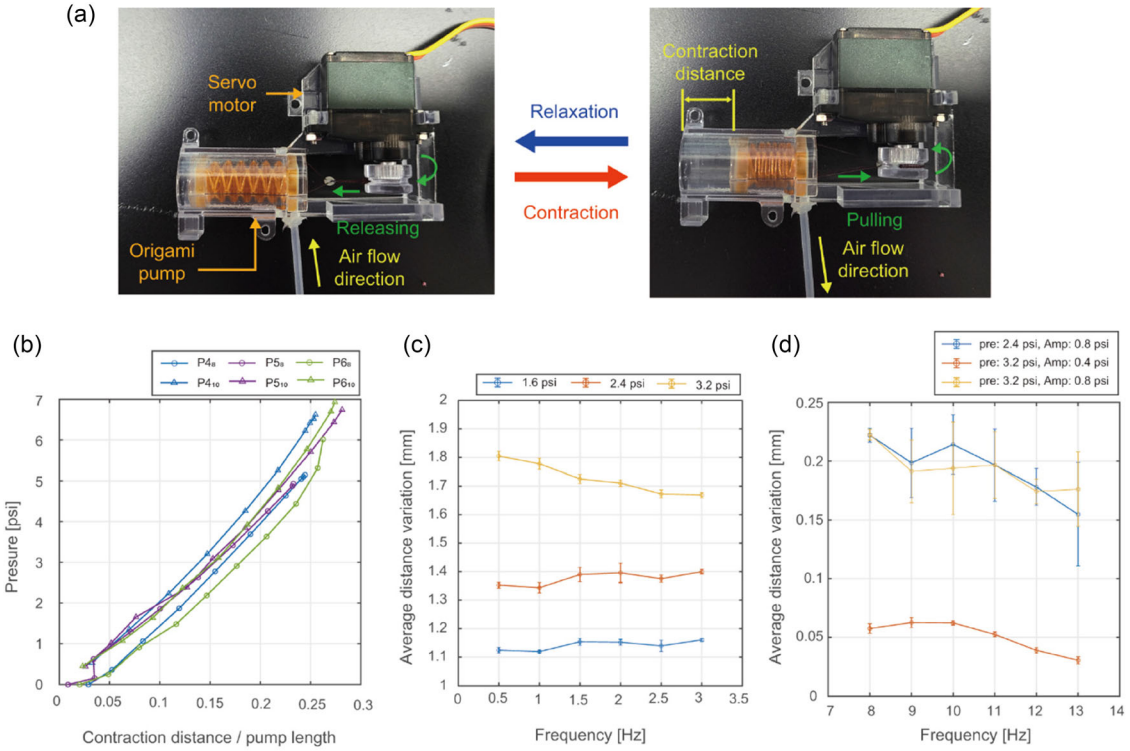

Figure 3. Designing of the OPM. a) Operation mechanism of the OPM. b) Pressure variations of the origami pump according to contraction ratio relative to the pump length. The blue, purple, and green colors showed the pressure variations of the 4th-, 5th-, and 6th-floor origami pumps, respectively. The circular and triangular markers represent the origami pattern width of 8 and 10 mm, respectively. c) Low-frequency responses of the origami pump from 0.5 to 3 Hz at 1.6, 2.4, and 3.2 psi pneumatic pressure with no preinjected pressure. d) High-frequency responses of the origami pump from 8 to 13 Hz for the different preinjected pneumatic pressure and variation in the pneumatic amplitude. The preinjected pneumatic pressure selected as 2.4 and 3.2 psi pneumatic pressure. The vibration amplitude in the pneumatic amplitude was 0.4 and 0.8 psi. The error bar represented the standard deviation.

relationship, we utilized the linear contraction range of the OPM to manipulate the SFP. When the servo motor rotated counterclockwise (increasing rotation angle direction), threads connected to the origami pump was pulled, causing the pump to contract. During the contraction of the pump, pneumatic pressure was generated and supplied to the actuator of the SFP. Conversely, when the servo motor rotated clockwise (decreasing rotation angle direction), the pump and actuator returned to its original state due to its resilience.

To determine design of the origami structure, pneumatic pressure was investigated according to contraction distances of the origami pumps. We tested six pumps characterized by different widths and floor of the Yoshimura origami pattern. Definitions and values of width and floors are described in Figure S3 and Table. S1, Supporting Information. The width was selected as 8 and 10 mm. Also, the floors of the pattern were chosen 4th, 5th, and 6th floors. The other origami pumps having different widths and floors were excluded due to difficulties in folding or achieving sealing. The pressure measurement results for six pumps are shown in Figure 3b. The graph showed pressure variations according to the contraction ratio relative to the pump length of the six Yoshimura origami pumps. From this graph, high maximum air pressure was observed as the width of the origami patterns increased. Meanwhile, the contraction rate and air pressure demonstrated a linear correlation, irrespective of the number of origami floors, but maximum pneumatic pressures did not exceed 7 psi. Since the origami pump has its own resilience, when the pneumatic pressure inside the pump reaches 7 psi, the resilience of the origami pump and the tension generated by the servo motor may be balanced to prevent the servo motor from further generating the air pressure. Additionally, from the graphs showing pressure according to contraction distance (Figure S4, Supporting Information), the longest contraction length at maximum air pressure was observed in the 6th-floor pump. The range of available long contraction lengths can contribute to the precise generation of tactile sensations by finely adjusting the pneumatic pressure injected into the actuator. As the 7 psi of pneumatic pressure was sufficient to enable the tactor to make contact with the skin surface, a 10 mm width of the 6th-floor origami pump was selected to generate various pressures for controlling the SFP.

With this selected pump, we also investigated the low- and high-frequency responses of the origami pump. At low frequencies, a laser sensor measured average expansion distance variations of the NA based on the pressure generated by the pump when the pressures were 1.6, 2.4, and 3.2 psi at speeds ranging from 0.5 to 3 Hz. For high frequencies, the NA was pre-pneumatically applied to facilitate observation, and the injected pneumatic pressure was varied to amplitudes of 0.4 or 0.8 psi. As illustrated in Figure 3c, the NA showed almost

constant expansion distance variations (1.14 ± 0.016 and 1.38 ± 0.021 mm at 1.6 and 2.4 psi, respectively) despite changing frequency, except for the 3.2 psi case (1.72 ± 0.051 mm). In the high-frequency responses shown in Figure 3d, when pre-pneumatic pressure was the same in advance and the amplitude was varied differently (represented by the red and yellow lines), the average distance variation was small at the change in pneumatic pressure of 0.4 psi. In the other case, when the magnitude of the pre-pneumatic pressure was different (represented by the blue and yellow lines), applying high amplitude variations in the pneumatic pressure resulted in a rapid decrease in the average distance variation as the frequency increased, regardless of the pre-pressure. However, we observed that the average distance variations at the high pre-pneumatic pressure were relatively alleviated compared to the low case based on their standard deviations. Thus, low-frequency vibration could be stably demonstrated through amplitude changes of ≈1.5 mm or less while high-frequency vibration was achieved with a high pre-pressure.

2.3. Virtual Reality Application with SFP and OPM

The proposed SFP was adapted to a virtual reality system to verify its ability to render multiple haptic feedback. In this application, we focused on slipping and vibrating stimuli through touch. **Figure 4** shows the rendering process of the haptic feedback in this entire system. For system integration, we used three SFPs and six OPMs. Specifically, one SFP was linked to two OPMs. Also, the SFPs were worn on three fingers (thumb, index, and middle), and the OPMs were attached to the forearm. Each SFP and combined OPM had velcro strips to be worn on a fingertip and forearm, respectively, as shown in Figure 1d. We demonstrated the use of both SFPs and OPMs together in this application, but OPMs could also be positioned separately in an external environment. From this perspective, when the haptic device was operated while only wearing three SFPs, the total weight of the haptic device was ≈6 g. Furthermore, the total weight of the device was ≈180 g when wearing both the SFP and OPM. Since the weight requirements for soft wearable devices at hand and other devices were lower than 0.5 and 3 kg, respectively, our device design satisfied those requirements.[62,63] With this setting, the SFP and OPM were operated using external power. Simultaneously, a virtual hand mimicked the hand motions of users using a hand-tracking device (Leap Motion Controller, Leap Motion, Inc., USA). With this virtual hand, the user could interact with virtual objects. In particular, the virtual reality sent a single byte of data composed of 4 flags depending on simulations and interaction states. The data was transmitted to a microcontroller unit (Arduino Uno), and it managed a motor control board (PCA 9685, Sunfounder, USA) by pulse width modulation (PWM) signals to generate pneumatic pressure suitable for haptic feedback. When the microcontroller unit operate the NA and SA, average latency times of each actuator were 19.76 and 25.94 ms, respectively, as depicted in Figure S5, Supporting Information. The detailed description of the flags and setting of the virtual reality is clearly stated in the Experimental Section.

Figure 5 shows six interactions between the virtual reality and our device (Movie S2–S7, Supporting Information). These virtual reality simulations consisted of five simulations for shear motions and one simulation for vibration feedback. To express continuous surface feeling in Case 1 of Figure 5a, the SFP repeated a cycle of generating shear force several times in a short period (Movie S2, Supporting Information). Sweeping the continuous floor simulation of Case 1 evaluates whether the haptic device can transfer a continuous sweeping feeling to the user. In contrast, sweeping the discontinuous floor simulation of Case 2 evaluates how the device can transfer a discontinuous feeling, as shown in Figure 5b. To express discontinuous feeling, the SFP

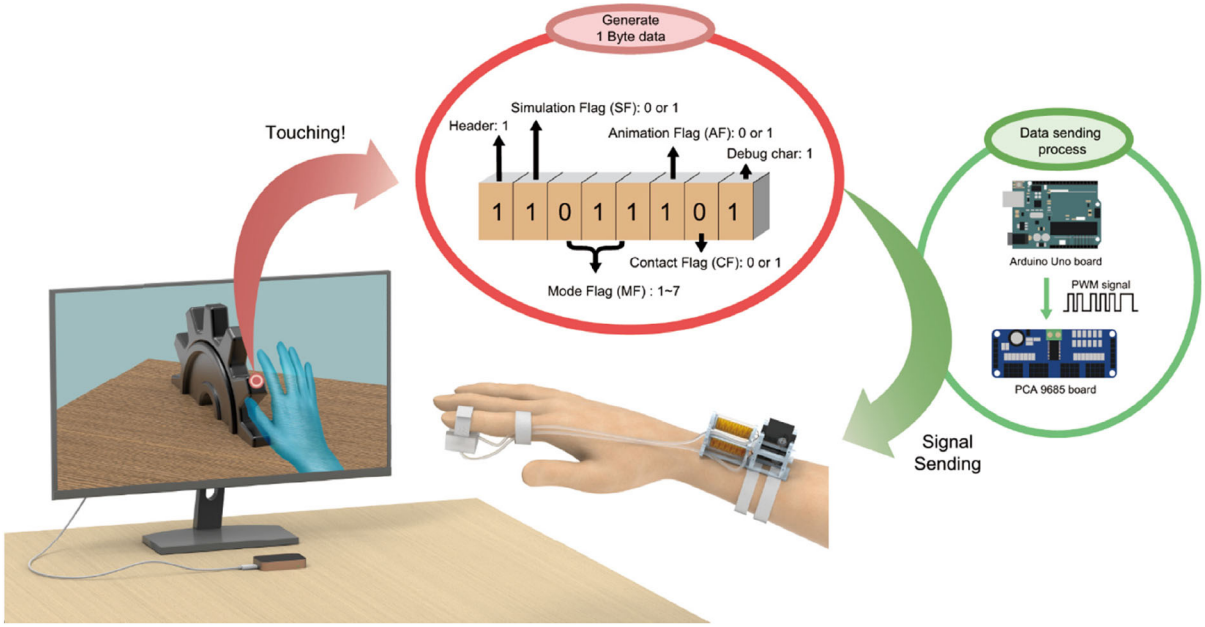

Figure 4. System configurations for operating the SFP and OPMs with virtual reality.

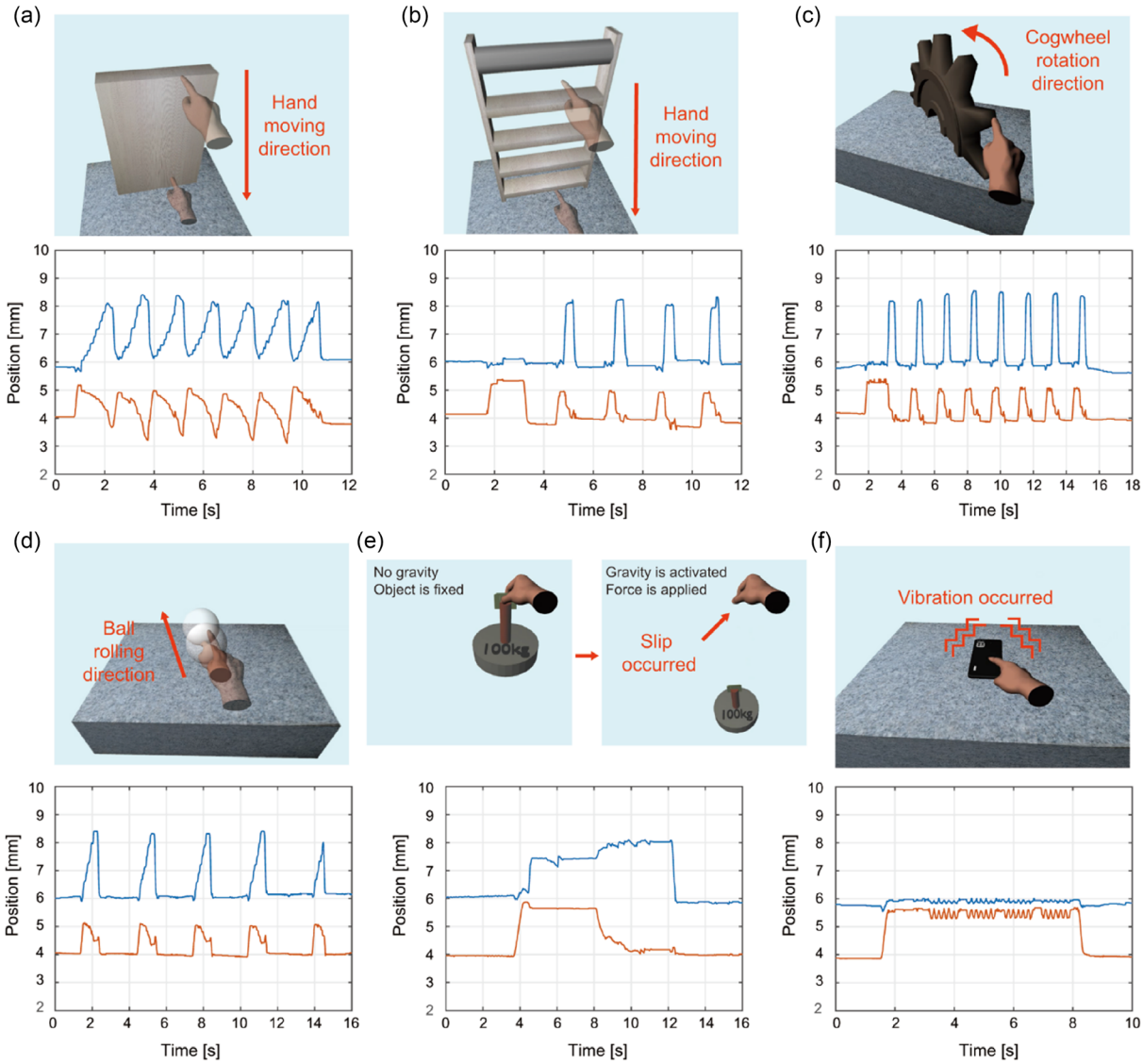

Figure 5. Demonstration of rendering tactile feedback using the SFP at six interactive simulations. The blue and red lines represent the tactor movements by the SA and NA, respectively. a) Case 1: Sweeping down the continuous surface object. b) Case 2: Sweeping down the discontinuous surface object. c) Case 3: Touching the finger on the rotating cogwheel. d) Case 4: Stroking the slippery ball. e) Case 5: Feeling the sensation of the heavy object falling. f) Case 6: Touching the vibrated cellphone.

operated one cycle when the virtual finger passes the discontinuous block (Movie S3, Supporting Information). In Case 3, a rotating cogwheel was designed to investigate whether moving animations enhance the tactile sensations experienced by users. When the users put their finger on the cogwheel teeth, the cogwheel moved to transmit the sweeping feeling to the user in Case 3, as shown in Figure 5c. The SFP actuates one cycle each time the teeth of the cogwheel hit the virtual finger (Movie S4, Supporting Information). To observe user responses when tactile feedback is provided during active engagement with virtual reality, we designed ball-rolling simulations in Case 4, as depicted in Figure 5d. While progressing through Case 4 simulation, the user experienced a sensation of the ball slipping when gently pressing on the ball with the SFP (Movie S5, Supporting Information). In Case 5, a falling object simulation was used to evaluate whether our device can accurately transfer the sensation of slipping between objects and fingers. This simulation embodied the sensation of catching a heavy object with two fingers and then missing it, as shown in Figure 5e. Herein, a key point was creating the sensation of an object slipping through the fingers. To create this feeling, the SA pushed the tactor while the air pressure of the NA was removed (Movie S6, Supporting Information). Finally, we configured the cell phone simulation to confirm the vibration implementation of the SFP in Case 6 (Figure 5f). In this simulation, the NA exerted 0.31 N to the finger of the user when the user touched the cell phone. After being touched, the NA started vibrating at a frequency of 6 Hz to transmit vibrations to the user when the cell

phone vibrated. In this simulation, forces of the NA varied between 0.2 and 0.3 N (Movie S7, Supporting Information). The operations of the interactive simulation are shown in Movie S8–S13, Supporting Information. The user moved their hand slowly up and down, keeping contact with the continuous board in Case 1 (Movie S8, Supporting Information). In Case 2, the users positioned their index finger on a cylinder. The cylinder changed to red in order to deliver contact information to the user visually. Afterward, the users moved their hand to sweep the discontinuous ladder with their index finger (Movie S9, Supporting Information). Meanwhile, the user did not move their hand after touching the cogwheel teeth in Case 3 (Movie S10, Supporting Information). When the hand maintained its position, the cogwheel rotated to transfer shear force to the finger. In Case 4, the user swept the ball, resulting in the ball rolling to the front (Movie S11, Supporting Information). Then, the shear force will be transferred to the user when they touch the rolling ball. In Case 5, the users pinched the heavy object with their thumb and index fingers before applying gravity. After pinching the object, we applied gravity to make it fall downward. From this simulation, the users could experience a slipping feeling between their hand and the object (Movie S12, Supporting Information). Lastly, the user contacted the cellphone, and the cellphone vibrated after the contact (Movie S13, Supporting Information). From this motion, the user experienced the vibration function of the SFP.

2.4. User Test

We evaluated the haptic feedback system through user test to investigate how users felt in each simulation.[64–66] Specifically, the user test was conducted with 20 participants (aged 20–28 years, 10 male and 10 female). We recruited participants in equal gender ratios to compare tactile perception between males and females.[67,68] Prior to proceeding with the test, the participants were asked about their previous experiences with virtual reality and haptic devices using the questions (Table S2, Supporting Information). The answers to these questions are shown in Figure S6a and Table S3, Supporting Information. Among them, a total of five participants (4 males and 1 female) answered that they had experience with the haptic device, and a total of seventeen participants (9 males and 8 females) had VR experience. In particular, the five participants who experienced the haptic device usually attempted to manipulate the device related to normal force or vibration. Hence, only one of the participants had previously used haptic devices that utilize shear forces.

In each test, three situations (no feedback, only normal force existed, and normal-shear forces existed) were tested to assess the performances of the SFP. These performances were scored by seven criteria between realism and artificiality.[52,53] The specific criteria and questions were demonstrated in Table S4, Supporting Information. **Figure 6**a shows the total user ratings for three situations. The three total scores were statistically analyzed using repeated measures ANOVA, and the feedback scores showed significant differences ($F(2,38) = 57.50$, $p < 0.001$). Additionally, post hoc pairwise comparisons were conducted to compare groups in pairs. According to comparison results, both "Only normal force" and "Normal & shear force" feedback conditions demonstrated significantly higher scores compared to the "No feedback" condition (Bonferroni pairwise comparisons; $p < 0.001$). "Normal & shear force" condition also showed a higher score compared to "Only normal force" (Bonferroni pairwise comparisons; $p < 0.001$). From these results, the participants felt much more realistic in situations when both normal and shear forces were exerted than in situations when no feedback or only normal force was exerted. Focusing on the normal-shear forces exerted situations at each interactive simulation as shown in Figure 6b, we confirmed that the SFP delivered participants a sense of reality as most of the user ratings were between 4 and 5. Specifically, the participants were better able to perceive slippery feelings in Case 3 and 4 simulations with the movement of virtual objects compared to Case 1 and 2 simulations without animation of virtual objects. From this result, we noticed that the SFP could be used more effectively when interacting with moving objects.[69,70] Moreover, in the case of vibration feedback related to the Case 6 simulation as shown in Figure 6c, the SFP could deliver an appropriate vibrating stimulus to the user. However, the scores between genders did not show significant differences. The specific results are presented in Table S5, Supporting Information.

Furthermore, the wearability of the device was surveyed among the participants, as illustrated in Figure S6b, Supporting Information. Based on the graph, the participants assessed that

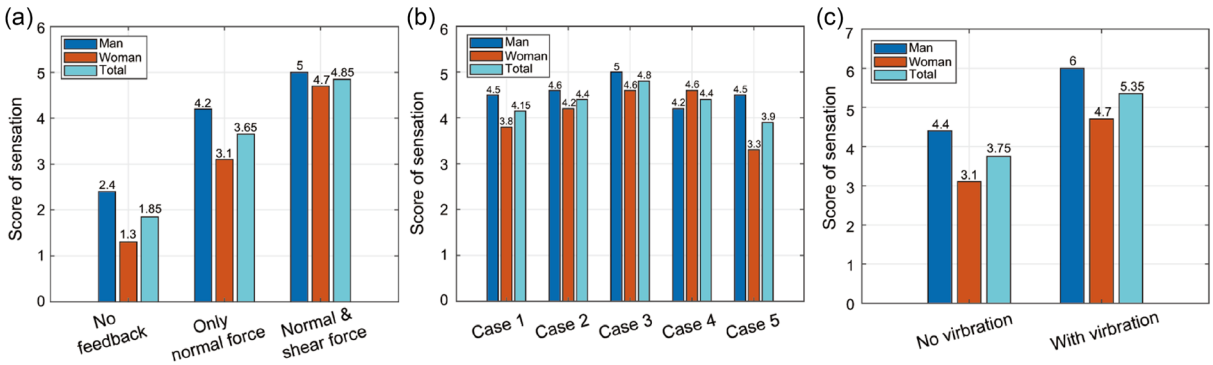

Figure 6. Results of the user test. A score of 0 to 7 represents a sense of reality and immersion. A score of 0 indicates that there is no sense of reality, and a score of 7 indicates that there is completely a sense of reality. a) Results from the 3 situations: no feedback, only normal force, and normal-shear forces. b) Results from the 5 interactive simulations related with shear force (Cases 1–5). c) Result from Case 6 for vibration test.

the device slightly limited hand movements, but it was tolerable when in use. Additionally, the female participants responded that they were more free to move their hands than the male participants. The evaluation criteria for wearability and detailed results are described in Table S6, Supporting Information.

3. Conclusion

In this study, we proposed the SFP with OPMs that was able to generate multiple feedback through pneumatic pressure. The comfortable and portable design overcame persistent problems with the pneumatic actuator applied to wearable devices (the bulky size and heavy weight) while still generating enough pneumatic pressure to operate the SFP. In addition, the SFP enabled the generation of normal force, shear force, and vibration through only two pneumatic actuators in a narrow area, improving wearability and versatility. The capabilities of the proposed device were demonstrated by comprehensive experimental studies. Furthermore, we conducted 5 virtual simulations involving shear forces to assess the haptic device's ability to effectively convey a complete sensory experience to the user. We demonstrated the feasibility and effectiveness of our device following the completion of qualitative user testing. Additionally, we confirmed that our haptic device can deliver vibrations effectively through the user study in Case 6. In this respect, the possibility of transmitting normal force, shear force, and vibration to the fingertips with the pneumatic actuators was validated. Furthermore, the SFPs were worn simultaneously on several fingers, as shown in Movie S14, Supporting Information. This movie presented one application which involved petting an animal using our device. By controlling each SFP differently, various forms of tactile feedback are selectively delivered to specific areas of contact. In this regard, teleoperation with a robot can be one application for our device.[71,72] When operating the robot hand, our device facilitates manipulation in areas obscured from view or inaccessible to direct human observation. In addition, the device can deliver dynamic situations such as touching objects with normal force, slipping objects with shear force, and hazard warning signals with vibration. Furthermore, this device can be used as an assistant tool in a robotic surgical system, owing to its capacity to generate complex feedback with small forces.[73] Since the possibility of wireless application with the light weight of our device was demonstrated, it can reduce the burden on surgeons by providing a delicate manipulation sensation. Additionally, due to the simple structures of the SFP and OPM, equipment transferring heat or sensors tracking hand motion can be integrated with our device. Further work will involve evaluating the SFP using quantitative assessments to enhance objectivity and generalizability. It will assign specific tasks that can utilize the device, and evaluate the speed and success rate of those tasks through user tests.[74] Also, electromyography signals will be used to assess whether the tactile feedback generated by the SFP is similar to the actual tactile feedback experienced by a human.[75]

4. Experimental Section

SFP Fabrication: The SFP was fabricated with two types of silicone of different hardness, Ecoflex (Ecoflex 0030, Smooth-On Inc., USA) and Sorta-Clear (Sorta-Clear 40, Smooth-On Inc., USA). The Ecoflex has a hardness of Shore 00-30 A and a curing time of 4 h at room temperature. This silicone was selected to use at the inflation part of the SFP because Ecoflex has high elongation properties. In the Sorta-Clear case, it has a hardness of Shore 40A and a curing time of 16 h at room temperature. The Sorta-Clear was selected to use at noninflation part of the SFP because it has a higher shore hardness than the Ecoflex. The Ecoflex part expanded more rapidly than the Sorta-Clear part, thereby restricting the expanding direction of the SFP as we had intended. To cure these silicone, silicone molds were 3D printed with acrylonitrile butadiene styrene (ABS) material. NA, SA, and tactor were fabricated separately and then combined into one as shown in Figure S7, Supporting Information. For the NA, Ecoflex mixture (mixed part A and B with ratio of 1:1) was cured as a square shape at room temperature for 4 h, and Sorta-Clear mixture (mixed part A and B with ratio of 100:10) was also cured as a square shape with a silicone hose to allow air to flow inside at room temperature for 16 h. The curing time of Ecoflex could vary depending on curing temperature, but this does not affect the performance of the SFP.[76] However, when we changed the curing temperature of Sorta-Clear to reduce curing time, it also changed the elongation of Sorta-Clear. After each part was sealed together using Sorta-Clear mixtures, the $15 \times 9 \times 2$ mm (W × D × H mm) bottom actuator was fabricated. Similarly, parts of the side actuator were fabricated separately and sealed together with a polyvinyl chloride (PVC) frame that limited expanding direction of the actuator as forward. The dimension of the side actuator was $15 \times 7 \times 5$ mm. These two actuators were attached together using Sorta-Clear to form a body of the SFP. During this process, velcro strips were inserted inside Sorta-Clear mixtures, and the mixture was cured simultaneously. The total body size was $15 \times 15 \times 10$ mm.

To fabricate the tactor, epoxy glue (3MScotch-Weld Epoxy Adhesive DP460) was cured with sliced velcro strips in a silicone mold at room temperature for 1 day. After the curing process, silicone mold was removed. For creating a wing of the tactor, the cured epoxy part was placed inside a mold to pour the Ecoflex. Finally, the SFP was completed by attaching the fabricated tactor and the body using cyanoacrylate adhesive with primer (AXIA-2700, Alteco Korea Inc., Korea). In addition, an arch-shaped upper part made by Sorta-Clear was placed on top of the side actuator. The fixation of the upper part was progressed using Sorta-Clear. The weight of the SFP was about 2.1 g. Photographs of the mold and each part are shown in Figure S8, Supporting Information.

Origami Pump Module Fabrication: An origami pump was fabricated by folding Yoshimura pattern that was carved on a 100 μm polyethylene terephthalate film (overhead projector (OHP) film, Copier Land Co., Ltd., Korea) using a laser cutter (Epilog Fusion Edge- RF30w, Epilog Laser Co., USA).[46,61] One side of the origami pump was sealed with a pump lid 3D printed by ABS. The pump lid had three holes to pass threads. Three threads were affixed at the pump lid. Subsequently, a pump frame was 3D printed using ABS to fix a servo motor (MG90D, Tower Pro Pte. Ltd.) and sealed with the other side of the origami pump. The origami pump was affixed at the pump frame with an outer pump frame using the epoxy glue. In addition, a pulley was 3D printed to fix threads. This pulley was connected to the motor. The threads passed through holes in the pump frame and attached themselves using the epoxy glue to prevent loosening. The threads were wound and tied to the pulley. Lastly, to transfer air pressure to the SFP, a silicone hose was connected to the origami pump using Sil-Poxy (Smooth-On Inc., USA). The size of the OPM was $68 \times 40 \times 15$ mm, and the weight was ≈60 g. To operate one SFP, two origami pump modules were assembled from each other. Moreover, velcro strips were attached to the pump module to wear it on a forearm. The schematic of the fabrication is shown in Figure S9, Supporting Information.

Measuring Pneumatic Pressure of the Origami Pump: The pneumatic variations and contraction distances were measured by a pressure sensor (33A-015D-2210, Shiba Korea Co., Ltd., Korea) and laser sensor (IL-100 CMOS multifunction analog laser sensor, Keyence Co., Japan). Each sensor was also connected with Arduino Uno and data acquisition board (DAQ) (DAQ NI-9229, National Instrument Co., USA) to collect sensor data simultaneously.

Setting Virtual Reality: Virtual interactive environment was made by 64-bit Openframeworks along Bullet Physics 2.81 for physics

simulation.[77,78] The virtual program was executed at 30 Hz on an Intel i7-10700 2.9 GHz CPU with 32 GB DDR4 2400 MHz. A portable hand tracking device (Leap Motion Controller, Leap Motion, Inc., USA) was used to make a virtual hand follow user hand motions simultaneously. The tracking device perceived the positions of hand joints. To utilize the tracking data, a virtual hand was created using 3D modeling software (Blender, Blender Foundation, Netherlands). Armatures were inserted at the joints of the virtual hand, and they connected with hand mesh. With the fabricated virtual hand, the hand was loaded into the virtual reality, and the position data obtained from the tracking devices was applied to each armature. The data was updated at a rate of 60 fps. Virtual objects were also created by the 3D modeling software and loaded into the virtual reality. To generate collision situations, bullet rigid shapes were inserted inside the virtual hand and objects depending on each shape. Moreover, these shapes followed movements of the virtual hand and objects. When collision states were changed due to collision between the bullet rigid shapes, one byte transmitting data was generated.

In the transmitting data, four flags existed depending on the states of the environment. The flags included simulation flag (SF), mode flag (MF), contact flag (CF), and animate flag (AF). SF determined the simulation situations of the SFP. When the SF was 0 or 1, the SFP generated only normal forces or both normal-shear forces. MF noticed simulation mode of the virtual environment, and CF detected touching between the virtual hand and objects. Lastly, AF indicated states of animations including cogwheel rotation, fall of the heavy object, and cellphone vibration. Before starting simulations, simulation situations and modes were selected through SF and MF. The tracking device tracked joints of the user hand and embodied a virtual hand in virtual reality. When the virtual hand contacted with the virtual objects, CF was changed to 1. Also, AF was changed depending on the executing animations of the objects. The virtual reality integrated these four flags with a header and debug char as one byte data and sent this flag to a microcontroller unit through serial communication at a rate of 9600 bps. This one byte data was transmitted only when changes in the flags were detected. The microcontroller (Arduinno Uno) decoded one byte data as pulse width modulation (PWM) signals and decoded data transmitted to a motor control board (PCA 9685, Sunfounder, USA) by serial peripheral interface (SPI) communication to control OPMs according to simulations. Lastly, when the OPMs were operated, the tactile feedback was transferred to the fingers of the user. The schematic is illustrated in Figure 4.

User Test with Participants: The user test for this study was approved by the Korea University Institutional Review Board (Approval Number: KUIRB-2024-0367-01). Twenty Korean participants in their 20*s* (10 male and 10 female) participated voluntarily in the test with informed consent. All participants were right-handed and had no restrictions on feeling the touch using their hands.

Supporting Information

Supporting Information is available from the Wiley Online Library or from the author.

Acknowledgements

This work was supported by the National Research Foundation of Korea (NRF) grant funded by the Ministry of Science and ICT (MSIT) (RS-2022-NR067595). The authors thank Jiwon Jung for helping draw the illustrations.

Conflict of Interest

The authors declare no conflict of interest.

Author Contributions

Jiyong Min and **Youngsu Cha**: proposed the research subject. **Jiyong Min**: designed the soft fingertip pneumatic devices. **Seongkwan Jang**: designed the origami pump module. **Jiyong Min** and **Seongkwan Jang**: conducted fabrication and experiments. **Jiyong Min** and **Seohu Lee**: constructed the virtual reality system and executed the user test. **Jiyong Min**: wrote the manuscript. **Youngsu Cha**: supervised the manuscript writing.

Data Availability Statement

The data that support the findings of this study are available from the corresponding author upon reasonable request.

Keywords

haptic devices, origami pumps, pneumatic actuators, shear forces

Received: April 1, 2025
Revised: May 29, 2025
Published online: June 26, 2025

[1] J. Psotka, *Instr. Sci.* **1995**, *23*, 405.
[2] S. Kavanagh, A. Luxton-Reilly, B. Wuensche, B. Plimmer, *Themes Sci. Technol. Educ.* **2017**, *10*, 85.
[3] G. S. Ruthenbeck, K. J. Reynolds, *J. Simul.* **2015**, *9*, 16.
[4] J. Lim, Y. Choi, *Electronics* **2022**, *11*, 1730.
[5] H. Kim, Y. T. Kwon, H. R. Lim, J. H. Kim, Y. S. Kim, W. H. Yeo, *Adv. Funct. Mater.* **2020**, *31*, 2005692.
[6] J. Yin, R. Hinchet, H. Shea, C. Majidi, *Adv. Funct. Mater.* **2020**, *31*, 2007428.
[7] A. Frisoli, D. Leonardis, *Nat. Rev. Electr. Eng.* **2024**, *1*, 666.
[8] A. Adilkhanov, M. Rubagotti, Z. Kappassov, *IEEE Access* **2022**, *10*, 91923.
[9] H. Fang, J. Guo, H. Wu, *Nano Energy* **2022**, *96*, 107112.
[10] Y. Lee, S. Lee, D. Lee, *Appl. Sci.* **2021**, *11*, 6932.
[11] K. Jung, S. Kim, S. Oh, S. H. Yoon, *Virtual Reality* **2024**, *28*, 13.
[12] A. Raza, W. Hassan, S. Jeon, *IEEE Access* **2024**, *12*, 59485.
[13] D. Prattichizzo, F. Chinello, C. Pacchierotti, M. Malvezzi, *IEEE Trans. Haptics* **2013**, *6*, 506.
[14] H. Kim, H. Yi, H. Lee, W. Lee, in *Proc. CHI Conf. Human Factors Computing Systems*, Vol. *501*, ACM, New York, NY **2018**, pp. 1–13.
[15] M. Gabardi, M. Solazzi, D. Leonardis, A. Frisoli, in *IEEE Haptics Symp. (HAPTICS)*, IEEE, Piscataway, NJ **2016**, p. 140.
[16] A. G. Perez, D. Lobo, F. Chinello, G. Cirio, M. Malvezzi, J. S. Martín, in *IEEE World Haptics Conf. (WHC)*, IEEE, Piscataway, NJ **2015**, pp. 327–332.
[17] D. Chen, A. Song, L. Tian, L. Fu, H. Zeng, *IEEE Trans. Haptics* **2019**, *12*, 281.
[18] M. A. Robertson, H. Sadeghi, J. M. Florez, J. Paik, *Soft Rob.* **2017**, *4*, 23.
[19] P. Moseley, J. H. Florez, H. A. Sonar, G. Agarwal, W. Curtin, J. Paik, *Adv. Eng. Mater.* **2015**, *18*, 978.
[20] S. Kanjanapas, C. M. Nunez, S. R. Williams, A. M. Okamura, M. Luo, *IEEE Rob. Autom. Lett.* **2019**, *4*, 1365.
[21] M. T. Thai, T. T. Hoang, P. T. Phan, N. H. Lovell, T. Nho Do, *IEEE Access* **2020**, *8*, 157878.
[22] Z. Sun, M. Zhu, X. Shan, C. Lee, *Nat. Commun.* **2022**, *13*, 5224.
[23] A. Gupta, M. O'Malley, *IEEE/ASME Trans. Mechatron.* **2006**, *11*, 280.
[24] S. Jeon, A. Talhan, *IEEE Access* **2017**, *6*, 3184.
[25] S. D. Laycock, A. M. Day, *Comput. Graph. Forum* **2003**, *22*, 117.

[26] K. T. Yoshida, C. M. Nunez, S. R. Williams, A. M. Okamura, M. Luo, in *IEEE World Haptics Conf. (WHC)*, IEEE, Piscataway, NJ **2019**, pp. 97–102.
[27] Y. Ujitoko, T. Taniguchi, S. Sakurai, K. Hirota, *IEEE Access* **2020**, *8*, 145107.
[28] H. Choi, S. Yoo, *Fashion Text.* **2023**, *10*, 31.
[29] A. Talhan, H. Kim, S. Jeon, *IEEE Access* **2020**, *8*, 957.
[30] Z. Zhakypov, A. M. Okamura, in *IEEE 5th Inter. Conf. Soft Robotics (RoboSoft)*, IEEE, Piscataway, NJ **2022**, pp. 938–944.
[31] Z. Ma, P. Ben-Tzvi, *J. Mech. Rob.* **2015**, *7*, 041008.
[32] A. Chortos, J. Liu, Z. Bao, *Nat. Mater.* **2016**, *15*, 937.
[33] Y. Zheng, D. Wang, Z. Wang, Y. Zhang, Y. Zhang, W. Xu, *Engineering* **2018**, *4*, 869.
[34] O. Ozioko, R. Dahiya, *Adv. Intell. Syst.* **2021**, *4*, 2100091.
[35] C. Pacchierotti, S. Sinclair, M. Solazzi, A. Frisoli, V. Hayward, D. Prattichizzo, *IEEE Trans. Haptics* **2017**, *10*, 580.
[36] C. Tawk, G. Alici, *Adv. Intell. Syst.* **2021**, *3*, 2000223.
[37] D. Kang, C.-G. Lee, O. Kwon, *Virtual Reality* **2023**, *27*, 1647.
[38] H. Shen, M. Zhou, Y. Chen, F. Xue, R. Su, *Flow Meas. Instrum.* **2024**, *100*, 102702.
[39] J. Zhao, T. Yu, Y. Zhang, H. Sun, M. Xu, *IEEE Rob. Autom. Lett.* **2024**, *9*, 7166.
[40] K. Iiyoshi, J. H. Lee, A. S. Dalaq, S. Khazaaleh, M. F. Daqaq, G. Korres, *IEEE Access* **2024**, *12*, 33309.
[41] D. Misseroni, P. P. Pratapa, K. Liu, B. Kresling, Y. Chen, C. Daraio, G. H. Paulino, *Nat. Rev. Methods Primers* **2024**, *4*, 1.
[42] M. A. Robertson, O. C. Kara, J. Paik, *Int. J. Rob. Res.* **2020**, *40*, 72.
[43] S. M. Felton, K. P. Becker, D. M. Aukes, R. J. Wood, *J. Micromech. Microeng.* **2015**, *25*, 085004.
[44] K. Lee, P.-G. Jung, Y. Cha, *IEEE/ASME Trans. Mechatron.* **2023**, *28*, 1436.
[45] Y. Kim, Y. Cha, *Front. Bioeng. Biotechnol.* **2020**, *8*, 00461.
[46] S. Seo, W. Park, D. Lee, J. Bae, *IEEE Rob. Autom. Lett.* **2021**, *6*, 5239.
[47] Z. F. Quek, S. B. Schorr, I. Nisky, W. R. Provancher, A. M. Okamura, *IEEE Trans. Haptics* **2015**, *8*, 209.
[48] M. Matscheko, A. Ferscha, A. Riener, M. Lehner, in *Inter. Symp. Wearable Computers (ISWC)*, IEEE, Piscataway, NJ **2010**, pp. 1–8.
[49] B. T. Gleeson, C. A. Stewart, W. R. Provancher, *IEEE Trans. Haptics* **2010**, *4*, 253.
[50] O. Kayhan, A. K. Nennioglu, E. Samur, in *IEEE Haptics Symp. (HAPTICS)*, IEEE, Piscataway, NJ **2018**, p. 26.
[51] P. Preechayasomboon, E. Rombokas, *Front. Virtual Reality* **2021**, *2*, 738613.
[52] P. Preechayasomboon, A. Israr, M. Samad, in *Proc. 2020 CHI Conf. Human Factors in Computing Systems*, ACM, New York, NY **2020**, pp. 1–13.
[53] M. L. Hammock, A. Chortos, B. C.-K. Tee, J. B.-H. Tok, Z. Bao, *Adv. Mater.* **2013**, *25*, 5997.
[54] B. B. Edin, G. K. Essick, M. Trulsson, K. A. Olsson, *J. Neurosci.* **1995**, *15*, 830.
[55] A. Girard, M. Marchal, F. Gosselin, A. Chabrier, F. Louveau, A. Lécuyer, *Front. ICT* **2016**, *3*, 00006.
[56] B. T. Gleeson, S. K. Horschel, W. R. Provancher, *IEEE Trans. Haptics* **2010**, *3*, 177.
[57] J. Qi, F. Gao, G. Sun, J. C. Yeo, C. T. Lim, *Adv. Sci.* **2023**, *10*, 2301044.
[58] H. E. Wheat, L. M. Salo, A. W. Goodwin, *J. Neurosci.* **2004**, *24*, 3394.
[59] M. Paré, H. Carnahan, A. M. Smith, *Exp. Brain Res.* **2002**, *142*, 342.
[60] Q. Zhang, H. Fang, J. Xu, *Front. Rob. AI* **2021**, *8*, 738214.
[61] S. Lee, S. Jang, Y. Cha, *iScience* **2024**, *27*, 111303.
[62] P. Polygerinos, Z. Wang, K. C. Galloway, R. J. Wood, C. J. Walsh, *Rob. Auton. Syst.* **2015**, *73*, 135.
[63] P. Aubin, K. Petersen, H. Sallum, C. Walsh, A. Correia, L. Stirling, *Int. J. Intell. Comput. Cybern.* **2014**, *7*, 233.
[64] J. Aldhous, E. Sobolewska, G. Webster, in *IEEE Inter. Conf. Metrology for eXtended Reality, Artificial Intelligence and Neural Engineering (MetroXRAINE)*, IEEE, Piscataway, NJ **2024**, pp. 243–248.
[65] M. Stamer, J. Michaels, J. Tümler, *HCI In Mobility, Transport, and Automotive Systems. Automated Driving and In-Vehicle Experience Design* (Ed: H. Krömker), Springer, Cham **2020**, pp. 404–416.
[66] G. García-Valle, M. Ferre, J. Breñosa, D. Vargas, *IEEE Access* **2017**, *6*, 7224.
[67] R. M. Peters, E. Hackeman, D. Goldreich, *J. Neurosci.* **2009**, *29*, 15756.
[68] A. Abdouni, M. Djaghloul, C. Thieulin, R. Vargiolu, C. Pailler-Mattei, H. Zahouani, *Royal Soc. Open Sci.* **2017**, *4*, 170321.
[69] Q. Tong, W. Wei, Y. Zhang, J. Xiao, D. Wang, *IEEE Trans. Haptics* **2023**, *16*, 154.
[70] T. Kassuba, C. Klinge, C. Hölig, B. Röder, H. R. Siebner, *NeuroImage* **2013**, *65*, 59.
[71] F. Kobayashi, G. Ikai, W. Fukui, F. Kojima, *J. Rob.* **2011**, *2011*, 419465.
[72] F. Abi-Farrajl, B. Henze, A. Werner, M. Panzirsch, C. Ott, M. A. Roa, in *IEEE/RSJ Inter. Conf. Intelligent Robots and Systems (IROS)*, IEEE, Piscataway, NJ **2018**, pp. 5010–5017.
[73] K. Zareinia, Y. Maddahi, C. Ng, N. Sepehri, G. R. Sutherland, *Int. J. Med. Rob. Comput. Assist. Surg.* **2015**, *11*, 486.
[74] H. Kim, M. Kim, W. Lee, in *Proc. 2016 CHI Conf. Human Factors in Computing Systems*, ACM, New York, NY **2016**, pp. 3694–3705.
[75] G. Li, L. Zhang, Y. Sun, J. Kong, *Multimed. Tools Appl.* **2019**, *78*, 29765.
[76] Z. Liao, M. Hossain, X. Yao, R. Navaratne, G. Chagnon, *Polym. Test.* **2020**, *86*, 106478.
[77] J. Min, T. Choi, Y. Cha, *Smart Mater. Struct.* **2023**, *32*, 035014.
[78] Y. Cha, J. Seo, J.-S. Kim, J.-M. Park, *Smart Mater. Struct.* **2017**, *26*, 057002.